V European Conference on Computational Fluid Dynamics
ECCOMAS CFD 2010
J. C. F. Pereira and A. Sequeira (Eds)
Lisbon, Portugal,14-17 June 2010

SPRAY DRAG MODEL FOR BLOODHOUND SSC SUPERSONIC VEHICLE

L. Remaki, B.J. Evans, O. Hassan and K. Morgan

School of Engineering,Swansea University,
Singleton Park SA2 8PP, Swansea, Wales, UK.
e-mail: L.Remaki@swansea.ac.uk, B.J.Evans@swansea.ac.uk, O.Hassan@swansea.ac.uk,
K.Morgan@swansea.ac.uk

Key words: Spray Drag, Fluid Dynamics, Gas-Particle, Riemann solver, Finite volume

Abstract. *This paper deals with the spay drag simulation for BLOODHOUND supersonic car. A gas-particle model is used to simulate the sand particles that rise because of the strong waveshoks-desert interaction. A finite volume scheme is used to discretise the continues model with a special treatment of the solid phase equations. Numerical tests are performed to analyze the impact of the sand particles on drag forces.*

1 INTRODUCTION

The BLOODHOUND SSC Project [1] was publicly announced in October 2008, with the objective of constructing a vehicle to take the World Land Speed Record to 1 000 mph, see for a prototype of the car. To successfully achieve this feat, many major technological problems will have to be overcome. The aerodynamic design of the vehicle is exclusively based on CFD simulations. This paper concentrates on one aspect, the study of the sand particles motion impact on the drag forces (Spay Drag). As BLOODHOUND SSC travels at supersonic speed, the shockwaves created around the body of the car interact with the surroundings disturbing the desert surface. This causes sand and dust particles to rise from the ground under the influence of pressure forces and these particles will then be moved up into the air by resistive drag forces. If there are enough particles in the air, then the air speed will be significantly affected. This could result in additional resistive forces acting on the car which are not typically accounted in CFD analysis. A Gas-Particle model is derived to simulate this impact. A typical continuity equation of volume fraction is solved as well as a momentum equation where drag forces and gravity are only considered. A finite volume method is used discretise the model with particle attention to the stability issue. Tests are performed on the old car model at supersonic speed of Mach=1.3, and the drag increase is clearly established.

Figure 1: Bloodhound SSC Supersonic Vehicle

2 GOVERNING EQUATIONS

The equations governing three dimensional unsteady viscous compressible flow are expressed over a fixed volume with a closed surface, in the integral form

$$\frac{\partial}{dt}(\phi_g\rho_g) + \nabla(\phi_g\rho_g U_g) = 0, \qquad \text{on } \Omega \times [o,T] \tag{1}$$

$$\frac{\partial}{dt}(\phi_g\rho_g U_g) + \nabla(\phi_g\rho_g U_g \otimes U_g) = -\nabla P_g + \nabla\tau_g - d_{fac}\frac{1}{\tau_p}\phi_g(U_g - U_p), \qquad \text{on } \Omega \times [o,T] \tag{2}$$

$$\frac{\partial}{dt}(\phi_p\rho_p) + \nabla(\phi_p\rho_p U_p) = 0, \qquad \text{on } \Omega \times [o,T] \tag{3}$$

$$\begin{aligned}\frac{\partial}{dt}(\phi_p\rho_p U_p) + \nabla(\phi_p\rho_p U_p \otimes U_p) = &-\frac{\phi_p}{\rho_p}\nabla P_g + d_{fac}\frac{1}{\tau_p}\phi_p(U_g - U_p) \\ &+\phi_p(1 - \frac{\rho_g}{\rho_p}), \qquad \text{on } \Omega \times [o,T]\end{aligned} \tag{4}$$

where ϕ_g, ϕ_p are the gas and particle volume fraction satisfying the conservation condition $\phi_g + \phi_p = 1$, $d_{fac} = \begin{cases} 1 + 0.15 R_{e_0}^{0.687} & \text{if } R_{e_0} < 1000 \\ 0 \quad \text{Else} \end{cases}$ is the drag coefficient, $R_{e_0} = \frac{D_p |U_p - U_g|}{\nu_g}$ is the particle Reynolds number, $\tau_p = \frac{\rho_p D_p^2}{18 \mu_g}$ is the particle response time and $\overrightarrow{g}$ is the gravity.

3 NUMERICAL DISCRETISATION

A finite volume method described below is used to discretise the overall gas-particle model. Equation is replaced by the non-conservative form to avoid dividing by zero when computing the velocity vector since the particle fraction volume variable takes zero value where the sand is absent. Therefore, the following equation is solved instead.

$$\frac{\partial}{dt}(U_p) + \nabla(U_p \otimes U_p) = -\frac{1}{\rho_p} \nabla P_g + d_{fac} \frac{1}{\tau_p}(U_g - U_p) + (1 - \frac{\rho_g}{\rho_p}), \qquad \text{on } \Omega \times [o, T] \qquad (5)$$

3.1 FINITE VOLUME METHOD

The domain Ω is discretised into a mesh of tetrahedral cells, using a Delaunay mesh generation process with automatic point creation [14, 15]. To enable the implementation of a cell vertex finite volume solution approach, a median dual mesh is constructed by connecting edge midpoints, element centroids and face centroids such that only one node is present in each control volume [14, 15]. Each edge of the grid is associated with a

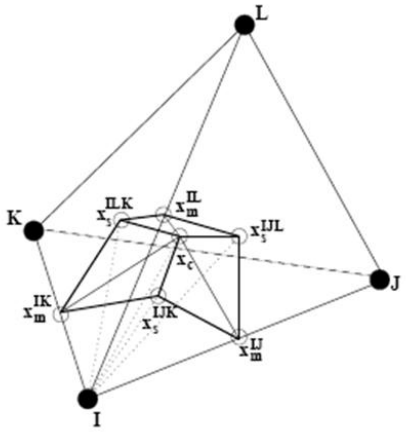

Figure 2: Illustration of that part of the dual mesh surrounding node I that is contained within a tetrahedral cell.

segment of the dual mesh interface between the nodes connected to the edge. The dual mesh interface inside the computational domain surrounding node I is denoted Γ_I. The lines which define the control volume interface surrounding node I are denoted byΓ_I^k.

The segment of the dual associated with an edge is a surface. This surface is defined using triangular facets, where each facet is connected to the midpoint of the edge, a neighboring element centroid and the centroid of an element face connected to the edge. This is illustrated in Figure 2. The midpoint of the edge between node I and J is termed x_m^{IJ}, the centroid of the face with vertices I, J and K is named and the element centroid is designated by x_c. The bold lines on the dual mesh in the figure illustrate the boundaries between the edges of which the dual mesh segment is associated. With this dual mesh

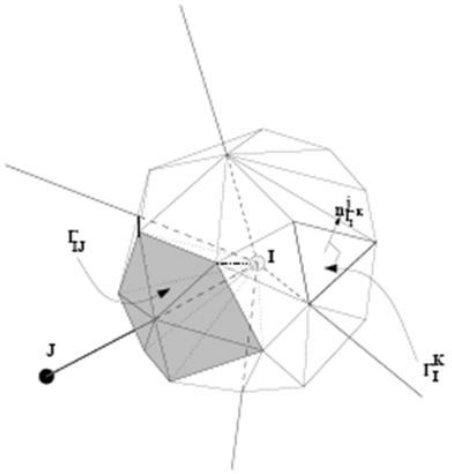

Figure 3: Illustration of the dual mesh surrounding an internal node I.

definition, the control volume can be thought of as constructed by a set of tetrahedra with base on the dual mesh. A complete dual mesh cell around an internal node I is shown in Figure 3.

Equation (10) is applied to each cell Ω_I of the dual mesh in turn. To perform the numerical integration of the inviscid fluxes over the surface $\partial\Omega_I$ of this cell, a set of coefficients is calculated for each edge using the dual mesh segment associated with the edge. The values of these coefficients for an internal edge are evaluated as

$$n_{IJ}^{\alpha} = \sum_{K \in \Gamma_{IJ}} A_{\Gamma_I^K} n_{\Gamma_I^K}^{\alpha} \tag{6}$$

where $A_{\Gamma_I^K}$ is the area of facet Γ_I^K and $n_{\Gamma_I^K}^{\alpha}$ is the component, in direction x_α, of the outward unit normal vector of the facet from the viewpoint of node I. The integral of the inviscid flux over the surface $\partial\Omega_I$ is then approximated as

$$\int_{\partial\Omega_I} \vec{F}^{\alpha} n^{\alpha} dS \approx \sum_{J \in \Lambda_I} \tilde{\vec{F}}_{IJ} \tag{7}$$

$$\tilde{\vec{F}} = \begin{pmatrix} \rho q_{IJ} \\ \rho u_1 q_{IJ} + p n_{IJ}^1 \\ \rho u_2 q_{IJ} + p n_{IJ}^2 \\ \rho u_3 q_{IJ} + p n_{IJ}^3 \\ (E+p) q_{IJ} \end{pmatrix} \tag{8}$$

is a consistent numerical flux function. The solution is advanced in time to steady state using an explicit multi-stage Runge Kutta procedure and the convergence is accelerated by the use of local time stepping and by the addition of an agglomerated multigrid process.

3.2 STABILIZATION AND FLUXES ESTIMATION

The HLLC solver with the limiter proposed in [24] is used for the fluid phase. A particular attention is payed to gas phase dicretisation. The momentum phase is stabilized by adding a first order artificial viscosity of the form

$$\triangle Q_i = \sum_{J \in N_I} \lambda_{IJ} \left(Q_J - Q_I \right) \tag{9}$$

With $\lambda_{IJ} = \frac{1}{1+tan(\theta_{IJ})^2}$, and θ_{IJ} is the angle between normal to the surface η_I and the velocity vector U_I. This allows diffusion to act only in the flow direction which minimize the cross wind effects as in streamline diffusion methods.

For the continuity equation, a Riemann problem for hyperbolic equation with discontinuous coefficients is solved to estimate the flux. The solution proposed in [24, 25] is considered, that is

Let's consider the following linear hyperbolic Riemann problem

$$\begin{aligned} \tfrac{\partial}{\partial t}\varphi + \beta(x)\tfrac{\partial}{\partial x}\varphi = 0, \qquad & \text{on } \Omega \times [o,T] \\ \varphi(0) = \begin{cases} \varphi_L & \text{if } x < 0 \\ \varphi_R & \text{if } x > 0 \end{cases} & \end{aligned} \tag{10}$$

Where β is a discontinuous function

The Riemann solution is then given by

$$\varphi(0,.) = \begin{cases} \varphi_L & \text{if } \beta_L > 0 and \beta_R > 0 \\ \frac{(\varphi_L + \varphi_L)}{2} & \text{if } \beta_L < 0 and \beta_R > 0 \\ \varphi_R & \text{if } \beta_L < 0 and \beta_R < 0 \\ \varphi_0 & \text{if } \beta_L > 0 and \beta_R < 0 \end{cases} \tag{11}$$

To estimate the flux in the finite volume discretisation of the continuity equation of particle volume fraction, the following equation is considered

$$\frac{\partial}{dt}(\phi_p) + q_{IJ}\frac{\partial}{ds}(\phi_p) = 0, \qquad \text{on } \Omega \times [o,T] \tag{12}$$

Where $q_{IJ} = U_p \eta_{IJ}$ and $U_p$is the particle velocity at node I and η_{IJ} is the normal to the surface separating dual cells associated with node I and J. The solution given above is used solve this equation.

3.3 BOUNDARY CONDITIONS

The classical viscous boundary conditions are imposed for the fluid phase and the slip condition is considered on the wall for the fluid phase. The particles fraction volume boundary condition on the ground is not obvious, however. The amount of particles (sand) that should be injected in the air and the area where they should released is not clear. In our case the variation of the pressure is considered as the principle cause of sand rising, therefore the gradient of particles velocity in the normal direction is selected as a criterion to define the sand rising area. More precisely particles are injected in the air if their normal to the ground velocity gradient is positive. Which means that particles are released if the pressure decreases just above the ground. As fore the quantity of sand to inject, we considered a reasonable constant value of 0.45, and by varying a bit this value we evaluate its effect on the variation of created drag. Figure 4 shows the delimited area obtained using the velocity gradient criterion.

4 NUMERICAL RESULTS

A sand particles risen by the flow around a supersonic Bloodhound car is simulated using the gas-particle model and the numerical scheme described in section 3. The imposed running conditions are M=1.3, AoA =0.0 and Re=13752000. The sand characteristics are $D = 0.08mm$ and $\rho_p = 1850kg/m^3$. A hybrid mesh is generated using FLITE package (described in for instance [14] and [15]). The mesh (5) contains 12384068 tetrahedral elements with a 12 prismatic layers. Figures 6 and 7 show the propagation of send particles around a wheel and around a car respectively. Figures 7 shows the drag convergence before and after send particle injection. The result shows a drag increase of 10%, which is reasonable and will not have a big effect on the car performance. Other tests (not provided in this work) are undertaken by varying the type of sand (size and density) and the volume fraction of sand released in the air from the ground in order to perform an accurate evaluation of the spray drag phenomenon.

5 CONCLUSIONS

- The paper presented a spray drag analysis using a gas-particle model to predict the impact of the sand particle risen from the ground because of shockwaves-ground interaction on the Bloodhound SSC supersonic vehicle. The model is dicretized using a finite volume scheme with the HLLC solver to estimate inviscid fluxes for the fluid, while a particular Riemann solver and oriented artificial viscosity are used to stabilize the solid fluxes. Preliminary results show an increase of 10% of drag. More tests are ongoing to show the effect of different type of sand in terms of size and density, the effect of the

fraction volume injected to the fluid on the drag variation. A deep analysis of the particles rising phenomenon is undertaken to attempt an accurate mathematical modelization.

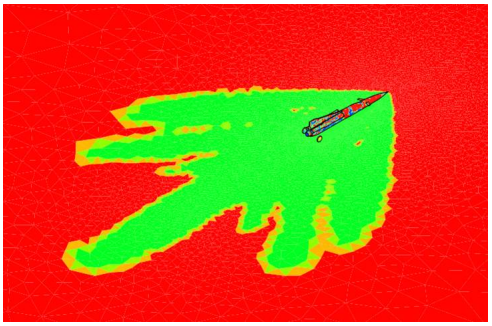

Figure 4: The delimited area using normal velocity gradient criterion

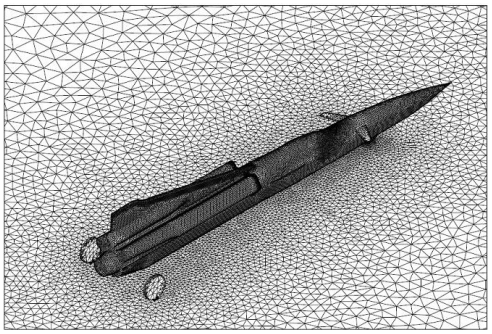

Figure 5: Bloodhound SSC Supersonic Car: Hybrid mesh

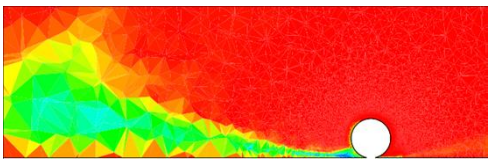

Figure 6: Sand particle propagation around a wheel

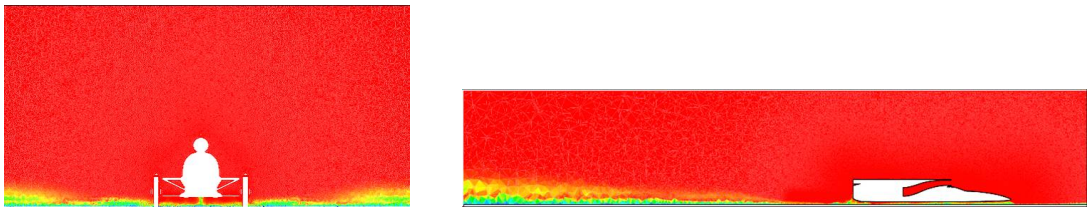

(a) (b)

Figure 7: Sand particle propagation around the vehicle: Frontal and Lateral cuts

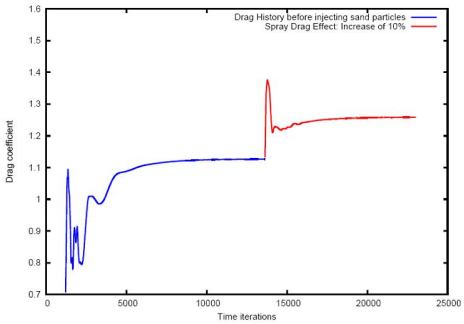

Figure 8: Spay Drag Effect: Drag convergence without and with sand particles coupling

REFERENCES

[1] L. Remaki, O. Hassan, K. Kenneth, A High Order Finite Volume-HLLC Solver and Anisotropic Delaunay Mesh Adaptation, *The 47th AIAA Aerospace Sciences Meeting and Exhibit. Orlando, Florida, USA*, 5 - 8 January 2009. AIAA-2009-1498.

[2] L. Remaki, M. Cheriet, Numerical Scheme of Shock Filter Models for Image Enhancement and Restoration, *Journal of Mathematical Imaging and Vision.*, **18**, 129–143 (2003).

[3] L. Remaki, Theoretical and numerical study of quasi-linear equations with discontinuous coefficients, and 2D linear acoustic, *PhD Thesis*, 1997, France.

[4] O. C. Zienkiewicz and R. C. Taylor, The finite element method, 4th Edition, *McGraw Hill*, **Vol. I** (1989), **Vol. II** (1991).

[5] S. Idelsohn and E. Oñate, Finite element and finite volumes, Two good friends, *Int. J. Num. Meth. Engng.*, **37**, 3323–3341 (1994).

[6] R. Abgrall, M. Ricchiuto, N. Villedieu, C. Tavé and H. Deconinck, Very High Order Residual Distribution On Triangular Grids, In proceedings of the *European Conference on Computational Fluid Dynamics*, ECCOMAS CFD 2006, P. Wesseling, E. Oñate and J. Periaux Eds., Egmond aan Zee, Netherlands, Paper n°583 (2006)

[7] V. Girault, P.–A. Raviart, Finite Element Methods for the Navier Stokes Equations, Springer, Berlin, 1986.

[8] A. Corsini, A FE Method for the Computational Fluid Dynamics of Turbomachinery, Lecture Notes, October 1999.

[9] R. Eymard, T. Galluöet, R. Herbin, Finite volume methods. Handbook of Numerical Analysis, North Holland, Amsterdam, 7:713-1020, 2000.

[10] C. Chainais–Hillairet, *Finite volume schemes for a nonlinear hyperbolic equation: convergence towards the entropy solution and error estimates*, M2AN Math. Model. Numer. Anal., 33(1999), 129–156.

[11] P–H. Cournède, C. Debiez, A. Dervieux, A positive MUSCL scheme for triangulations. INRIA Report 3465, 1998.

[12] J. A. Desideri, A. Dervieux, Compressible flow solvers using unstructured grids. Von Karman Institute Lecture Notes 1988–05, Von Karman Institute for Fluid Dynamics, Belgium, 1988.

[13] R. E. Ewing, T. Lin Y. and Lin, *On the accuracy of the finite volume element method based on piecwise linear polynomials*, SIAM J. Numer. Anal., 39(2002), 1865–1888.

[14] K. A. Sørensen, O. Hassan, K. Morgan, N. P. Weatherill, *A multigrid accelerated time–accurate inviscid compressible fluid flow solution algorithm employing mesh movement and local remeshing*, Int.J.Num.Meth.Fluids, 45(2003), 517–536.

[15] N. P. Weatherill, O. Hassan, K. Morgan, J. W. Jones, B. G. Larwood, K. A. Sørensen, *Aerospace simulations on parallel computers using unstructured grids*, Int.J.Num.Meth.Fluids, 40(2002), 171–187.

[16] E. F Toro, M. Spruce, W. Speares, *Restoration of the contact surface in the HLL–Riemann Solver*, Shock Waves, 4(1994), 25–34.

[17] E. F. Toro, Riemann Solvers and Numerical Methods for Fluid Dynamics, A Practical Introduction (2nd edn), Springer, Berlin, 1999.

[18] S. Taasan, D. M. Nark, An absorbing buffer zone technique for acoustic wave propagation, AIAA Paper 95–0146, 1995.

[19] J. Peraire, J. Peri, K. Morgan, *Adaptive remeshing for three–dimensional compressible flow computation*, J.Comp.Phys., 103(1992), 269–285.

[20] W. G. Habashi, J. Dompierre, Y. Bourgault, D. Ait–Ali–Yahia, M. Fortin, M–G. Vallet, *Anisotropic mesh adaptation: towards user–independent, mesh–independent and solver–independent CFD solutions. Part I: general principles*, Int.J.Num.Meth.Fluids, 32(2000), 725–744.

[21] E. F. D'Azevedo, R. B. Simpson, *On optimal triangular meshes for minimizing the gradient error*, Nm.Math., 59(1991), 321–348.

[22] M. Fortin, *Anisotropic mesh adaptation through hierarchical error estimators*, SIAM J.Numer.Anal., 26(1998), 788–811.

[23] V. Dolejsi, J. Felcman, Anisotropic mesh adaptation for transonic and supersonic flow simulation, in Proceedings of ALGORITMY Conference on Scientific Computing, 78–85 2002.

[24] L. Remaki, W. G. Habashi, *3–D mesh adaptation on multiple weak discontinuities and boundary layers*, SIAM J.Sci.Comput., 28(2006), 1379–1397.

[25] L. Remaki, C. Lepage, W. G. Habashi, Efficient anisotropic mesh adaptation on weak and multiple shocks, AIAA Paper 2004–0084, 2004.

[26] D. J. Mavriplis, Revisiting the least–squares procedure for gradient reconstruction on unstructured meshes, AIAA Paper 2003–3986, 2003.